

A Novel Organic “Polyurea” Thin Film for Ultralong-Life Lithium-Metal Anodes via Molecular-Layer Deposition

Yipeng Sun, Yang Zhao, Jiwei Wang, Jianneng Liang, Changhong Wang, Qian Sun, Xiaoting Lin, Keegan R. Adair, Jing Luo, Dawei Wang, Ruying Li, Mei Cai,* Tsun-Kong Sham,* and Xueliang Sun*

Metallic Li is considered as one of the most promising anode materials for next-generation batteries due to its high theoretical capacity and low electrochemical potential. However, its commercialization has been impeded by the severe safety issues associated with Li-dendrite growth. Non-uniform Li-ion flux on the Li-metal surface and the formation of unstable solid electrolyte interphase (SEI) during the Li plating/stripping process lead to the growth of dendritic and mossy Li structures that deteriorate the cycling performance and can cause short-circuits. Herein, an ultrathin polymer film of “polyurea” as an artificial SEI layer for Li-metal anodes via molecular-layer deposition (MLD) is reported. Abundant polar groups in polyurea can redistribute the Li-ion flux and lead to a uniform plating/stripping process. As a result, the dendritic Li growth during cycling is efficiently suppressed and the life span is significantly prolonged (three times longer than bare Li at a current density of 3 mA cm^{-2}). Moreover, the detailed surface and interfacial chemistry of Li metal are studied comprehensively. This work provides deep insights into the design of artificial SEI coatings for Li metal and progress toward realizing next-generation Li-metal batteries.

Li-ion batteries (LIBs) have been commercialized over the past decades and utilized for many applications, such as portable electronic devices and electric vehicles (EVs). However, the conventional LIBs cannot meet the increasing demands for high energy density storage systems, particularly long-distance EVs.^[1] Li-metal batteries (LMBs), as promising

alternatives to next-generation batteries, have attracted extensive attention due to their high energy density and low cost. Metallic Li is considered as the ultimate choice of anode material for LMBs, owing to its ultrahigh theoretical capacity (3860 mAh g^{-1}) and lowest electrochemical potential (-3.04 V vs the standard hydrogen electrode),^[2] LMBs were pioneered during the 1970s, but they have not been successfully commercialized due to the significant safety concerns^[3–5] associated with Li-dendrite growth during the repeated Li plating/stripping process. The challenges of commercial application of metallic Li anodes can be summarized as follows: 1) Li tends to deposit unevenly to form dendritic and mossy-like morphology on the electrode during electrochemical cycling, which can subsequently penetrate the separator and cause internal short-circuits and thermal runaway. The dendritic Li could also be


isolated from the bulk Li or current collector during the stripping process, becoming “dead Li” due to the absence of electronic contact, which leads to increased resistance, fading capacity, and short cycle life.^[6] 2) The side reaction between Li and liquid electrolyte results in the formation of a solid electrolyte interphase (SEI) layer on the electrode surface. The unstable SEI layer is very fragile and easily fractured during the Li plating/stripping process. As a result, fresh Li is exposed and further consumes more electrolyte to form new SEI. This repetitive process endlessly consumes both Li and electrolyte, leading to growing interfacial resistance and decreasing Coulombic efficiency (CE).^[7] 3) Owing to its “hostless” nature, Li metal undergoes a relatively infinite volume change during electrochemical cycling. This phenomenon causes significant challenges as it can often cause damage to the SEI during plating/stripping.^[3]

Among all the challenges of the Li-metal anode, the SEI plays a crucial role as a passivation layer to prevent further reactions between Li and electrolyte, hence improving electrochemical performance. A self-formed SEI is generally composed of the stacking of many small domains, including LiF, Li₂O, Li₂CO₃, and organic Li compounds, with heterogeneous composition, ionic conductivities, and mechanical properties.^[8] However, the deposition of dendritic or mossy-like Li still occurs during

Y. Sun, Y. Zhao, J. Liang, C. Wang, Dr. Q. Sun, X. Lin, K. R. Adair, J. Luo, Dr. D. Wang, R. Li, Prof. X. Sun
Department of Mechanical and Materials Engineering
University of Western Ontario
London, Ontario N6A 5B9, Canada
E-mail: xsun@eng.uwo.ca

J. Wang, Prof. T.-K. Sham
Department of Chemistry
University of Western Ontario
London, Ontario N6A 5B7, Canada
E-mail: tsham@uwo.ca

Dr. M. Cai
General Motors R&D Center
Warren, MI 48090-9055, USA
E-mail: mei.cai@gm.com

 The ORCID identification number(s) for the author(s) of this article can be found under <https://doi.org/10.1002/adma.201806541>.

DOI: 10.1002/adma.201806541

cycling because of the instability of the SEI layer under nonuniform Li-ion flux in inhomogeneous electric field. To date, massive efforts have been made to develop a robust artificial SEI layer for Li-metal anodes by different strategies, which can be categorized into in situ and ex situ SEI formations.^[9] In situ formation of a stable SEI can be realized by the modification of electrolyte composition. For example, the synergistic effects between LiNO₃ and Li polysulfide promote the formation of a double-layer SEI to passivate the Li surface and prevent further decomposition of electrolyte.^[10] Ex situ SEI layers are developed by creating artificial protective films on Li metal prior to cell assembly. Various types of coatings have been investigated, including metal oxides,^[7] solid state electrolytes,^[11] and polymeric films.^[6,12]

The fabrication of uniform protective coatings with controllable thickness remains challenging. The high chemical reactivity and low thermal stability of Li metal hinder the use of conventional chemical vapor deposition or wet chemical methods. With the unique features of low deposition temperature, high conformity, and precise control over thickness, atomic layer deposition (ALD) is an ideal technique to fabricate high-quality protective coatings for Li-metal anodes.^[13] ALD Al₂O₃ has been reported as a robust artificial SEI for both Li and Na electrodes to extend the lifetime and reduce the dendrite growth.^[14,15] Nevertheless, the brittle metal oxide films produced by ALD are unable to relieve the volume change and can be fractured during cycling. As an analogue of ALD, molecular-layer deposition (MLD) is a technique that can fabricate thin polymeric films by surface-limited reactions.^[16] It has several unique advantages, including design flexibility, tunable electrical properties, and mild deposition conditions.^[17] MLD fabrication can be classified into two categories: pure polymer-based organic films and metal-based inorganic-organic hybrid materials. Elam's group and our group have previously demonstrated alucone coatings, the most popular metal-based hybrid MLD film, for Li or Na metal anodes, showing improved stability over the inorganic Al₂O₃ coatings due to the improved flexibility from C–C and C–O bonds in alucone films.^[7,14,18] However, the alucone coating was only proved to mechanically suppress the dendrite growth without any evidence to direct a uniform Li-ion flux to the surface of the electrode. Meanwhile, there is no report on the fabrication of pure polymer thin films on battery materials for LIBs and LMBs through vapor-phase deposition techniques.

Herein, for the first time, we report a novel ultrathin organic film of “polyurea” via MLD as protective layer for Li-metal anodes to improve the cycle life and stability. This electrically nonconductive film can confine the Li deposition beneath the film and suppress the dendrite growth as a protective barrier. Meanwhile, as reported from simulations, the nitrogen-containing polar groups in polyurea can effectively regulate the Li-ion flux and lead to a uniform Li deposition (Figure 1a).^[19] Owing to these functions, the Li-metal anode coated with polyurea layer enables greatly prolonged lifetime in the symmetric cells at different current densities and capacities. The full cells were tested using LiFePO₄ (LFP) as the cathode and showed improved capacity retention and rate performance. Therefore, this work sheds new light on the design of protective layer for Li-metal anodes to achieve long lifetime and high cyclability.

The polyurea thin films were coated on ≈250 μm fresh Li foils by alternatively introducing ethylenediamine (ED) and 1,4-phenylene diisocyanate (PDIC) to form urea bond linkages, following our previous work (Figure 1a).^[20] Quartz crystal microbalance (QCM) was applied to study the film growth behavior in situ (Figure S1, Supporting Information). From the QCM data, it is confirmed that the deposition is a MLD process following a sequential and stepwise reaction manner with a stable mass gain of ≈24 ng cm⁻² from a pulse of PDIC and ≈11 ng cm⁻² from ED. To optimize the coating thicknesses, different number of cycles (5, 10, 25, and 50 cycles) were carried out on Li foils and denoted as Li@P5, Li@P10, Li@P25, and Li@P50, respectively. From the scanning electron microscopy (SEM) images, compared with bare Li, Li@P10 exhibited a rougher appearance on the surface, which indicates the deposition of polymeric coating (Figure S2, Supporting Information). X-ray diffraction analysis showed peaks at 36.1°, 51.9°, and 64.9°, corresponding to Li crystal for both bare Li and Li@P10 after subtracting the signals of the sample holder (Figure S3, Supporting Information). No peaks from polyurea film were detected because of its amorphous nature and nanometer scale. For the information on polyurea film, time-of-flight secondary ion mass spectrometry (TOF-SIMS) was used to identify the distribution and depth profiles of various elements and molecular moieties on the outermost surface. Figure 1b–d presents the TOF-SIMS results and corresponding depth profiles for Li@P10. Secondary ions from hydrocarbon (C₂H⁻, C₄H⁻, and C₆H⁻) and urea (CN⁻ and NCO⁻) were detected with strong signals in the observed area, while very weak signal was detected from Li⁻ (as shown in Figure 1b), suggesting that the surface of Li was fully covered by the polyurea film with only 10 MLD cycles. Moreover, a high ratio of ≈40% in counts of C₆H⁻ to C₂H⁻ was detected, indicating the presence of benzene rings from the PDIC precursor.^[21] To obtain the elemental mapping beneath the outermost surface, a square area in the center with a depth of ≈4 nm was removed by Cs⁺ sputtering for 40 s. It should be mentioned that the depths in TOF-SIMS can be estimated by multiplying sputtering time with sputtering rate (≈0.1 nm s⁻¹). As shown in Figure 1c, in the center square area, the signal of Li increased dramatically from ≈6000 to ≈34 000 counts, whereas the signal from hydrocarbon and urea showed a large decrease. The trends for the change of secondary ions were also confirmed by depth profiles, in which the content of Li was almost zero at outermost surface and eventually becomes higher than the hydrocarbon after sputtering for 40 s (Figure 1d). The content of NCO⁻ was low within 5 s of sputtering time due to the reaction with atmosphere on the surface during sample transfer. It can be inferred that the thickness of 10 MLD cycles of polyurea film on Li metal is ≈4 nm, because the contents of both hydrocarbon and urea dropped gradually with depth and leveled after 40 s (Figure 1d). TOF-SIMS was also conducted for Li@P25 and Li@P50 (Figure S4, Supporting Information). Similarly, stronger signals from polyurea and weaker signals from Li were detected on the outermost surface upon increasing cycle numbers. Therefore, higher cycle numbers result in a denser and much more compact polymeric film. From the depth profiles for Li@P25 and Li@P50 (Figure S4c,f, Supporting Information), it can be inferred that the polyurea films become thicker with increasing MLD cycles,

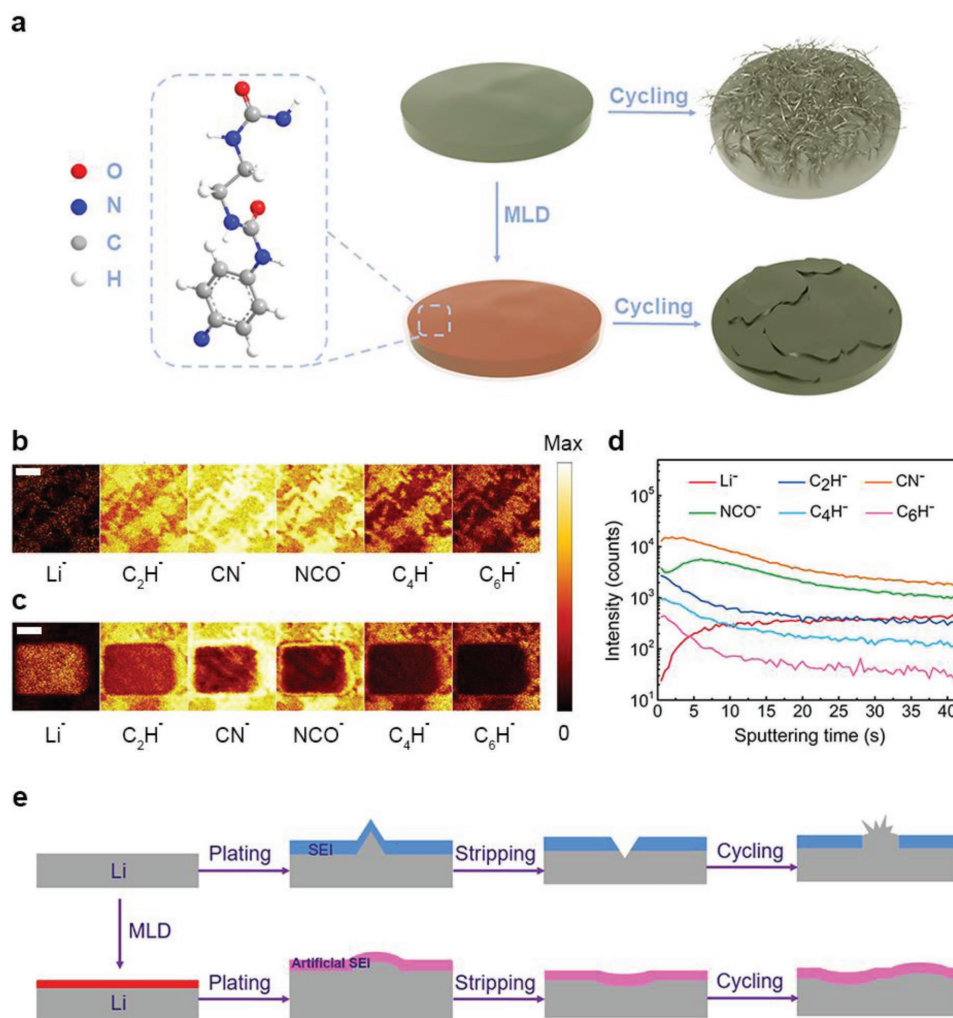


Figure 1. An illustration of polyurea coating on Li electrodes. a) Schematic diagrams showing the effect of MLD coating on a Li anode when cycling. b,c) TOF-SIMS secondary ion images of Li@P10 before (b) and after (c) Cs⁺ consecutive sputtering for 40 s (the length of scale bar is 100 μ m). d) Depth profile of various secondary ion species obtained by sputtering. e) A comparison of Li plating/stripping on bare Li and polyurea-coated Li.

because the signals of secondary ions that are generated from polymer continue to decrease to ≈ 8 and ≈ 12 nm, respectively. X-ray photoelectron spectroscopy (XPS) was also conducted to confirm the surface composition of Li@P10 (Figure S5, Supporting Information). In the O 1s spectrum, the peaks at 533.1 and 531.3 eV corresponded to C–O and C=O bonds, respectively. The N 1s spectrum with the peaks at 400.2 and 397.8 eV indicated amide/amine and N=C structures, and the C 1s spectrum confirmed the presence of carbon–carbon, hydrocarbon, and carbon–oxygen bonds, which are consistent with the structures of polyurea film and its end group from precursors. The cross-section SEM image for 100 cycles of MLD polyurea film on Si wafer showed ≈ 40 nm thickness and energy-dispersive X-ray spectroscopy mapping also confirmed homogeneous distributions of C, N, and O elements, further indicating the uniformity of the polyurea coating via MLD process (Figures S6 and S7, Supporting Information). The MLD growth rates for polyurea on Si and Li are similar at ≈ 0.4 nm per cycle, which are comparable with previously reported values from the literature.^[20,22]

To evaluate the influence of polyurea coatings on the electrochemical performance of Li-metal anodes, symmetric 2032-type coin cells were assembled using either polyurea-coated Li foils (Li@P10) or bare Li foils in commercial carbonate electrolyte (1 M LiPF₆ dissolved in 1:1:1 ethylene carbonate (EC)/diethyl carbonate (DEC)/dimethyl carbonate (DMC)). **Figure 2a** demonstrates the potential profiles of bare Li and Li@P10 at a constant current density of 1 mA cm⁻² with a capacity limit of 1 mAh cm⁻². The plating/stripping overpotential of bare Li was initially maintained at ≈ 110 mV (vs Li⁺/Li) and gradually increased to ≈ 730 mV after 360 h. Subsequently, a sudden drop in overpotential was detected, followed by fluctuation, which could be explained as the internal soft shorting of the cell due to the Li-dendrite formation. By contrast, Li@P10 showed improved stability and longer cycling life without any sign of soft shorting (Figure 2b–d). The overpotential of Li@P10 was initially similar to bare Li, but stably remained without showing any significant increase for more than 460 h. The improvement of cycling performance can be attributed to the more stable SEI and uniform Li-ion flux directed by polyurea films. Remarkably,

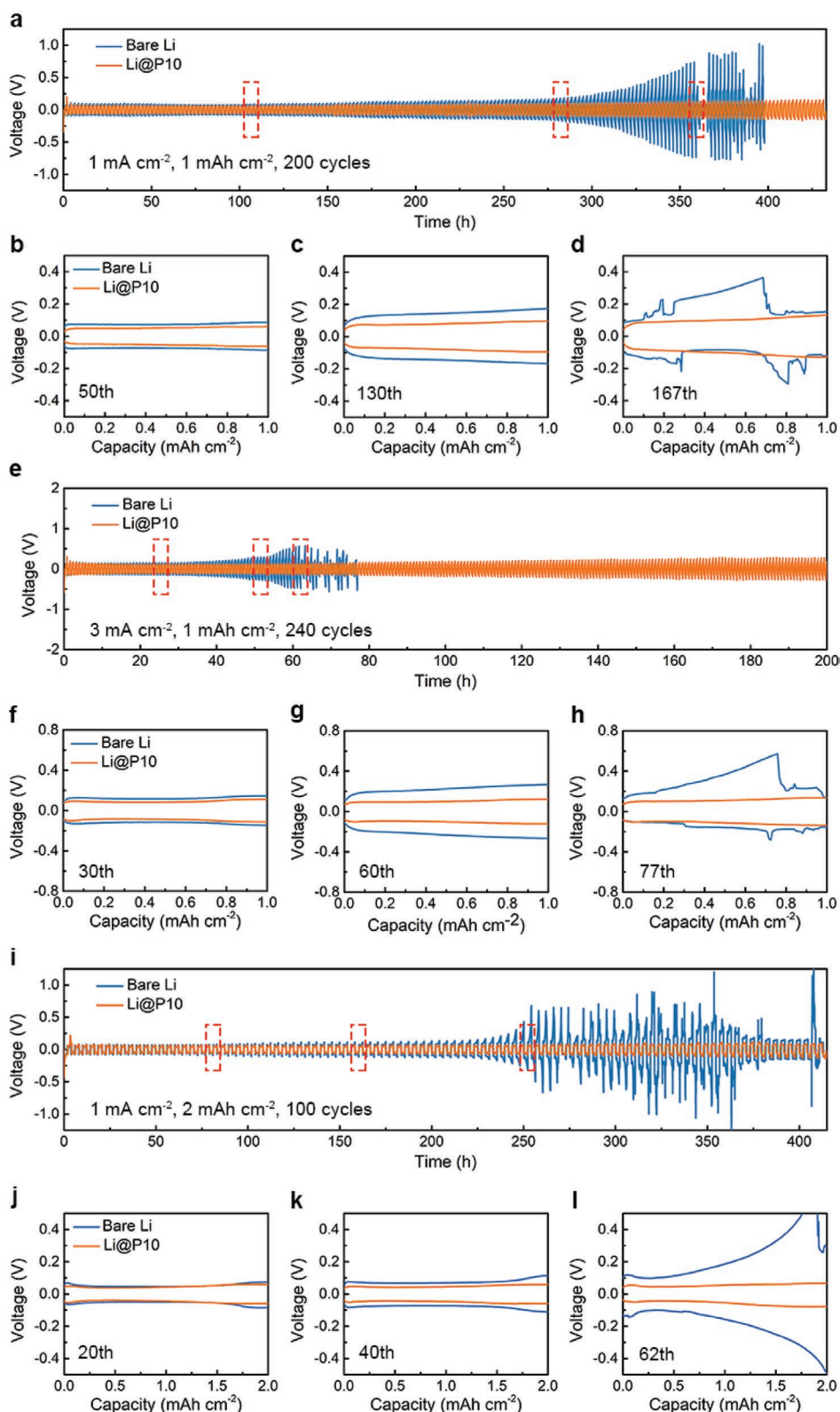


Figure 2. Electrochemical performance of symmetric cells using Li@P10 anodes. a) Galvanostatic cycling profile of bare Li and Li@P10 with a current density of 1 mA cm^{-2} and capacity of 1 mAh cm^{-2} . b–d) Detailed voltage profiles at 1 mA cm^{-2} for: b) 50th, c) 130th, and d) 167th cycles. e) Corresponding profile at a higher current density of 3 mA cm^{-2} for the capacity of 1 mAh cm^{-2} . f–h) Detailed voltage profiles at 3 mA cm^{-2} for: f) 30th, g) 60th, and h) 77th cycles. i) Corresponding profile at a current density of 1 mA cm^{-2} for a higher capacity of 2 mAh cm^{-2} . j–l) Detailed voltage profiles for: j) 20th, k) 40th, and l) 62th cycles for the capacity of 2 mAh cm^{-2} .

the polyurea protective layer indicated stronger capability at higher current densities. When increasing the current density to 3 mA cm^{-2} , the overpotential of bare Li was $\approx 180 \text{ mV}$ in the initial cycles and rapidly increased to $\approx 570 \text{ mV}$ within 65 h (Figure 2f–h). Subsequently, the failure of the cell occurred in only 62 h, due to the rapid growth of Li dendrites, which penetrated the separator (Figure 2e). Promisingly, the overpotential of Li@P10 showed a slight decrease to 135 mV within the initial 65 h, indicating a highly stable Li stripping/plating process. The cell using Li@P10 can operate with minor change in overpotential for over 240 cycles ($\approx 200 \text{ h}$), which is more than three times longer life span than that of bare Li. For more practical applications, higher capacity of 2 mAh cm^{-2} has been further investigated. When increasing the capacity to 2 mAh cm^{-2} , the Li@P10 still showed enhanced electrochemical performance than bare Li, for more than 100 stripping/plating cycles with overpotentials lower than 100 mV (Figure 2i). By contrast, a sharp overpotential increase from ≈ 80 to $\approx 700 \text{ mV}$ occurred in 65 cycles for bare Li followed by an immediate cell failure (Figure 2j–l). When cycling at a high current density of 5 mA cm^{-2} , the overpotential of the cell using Li@P10 at the beginning was much lower and stable than that using bare Li from the voltage profile (Figure S8, Supporting Information). It operated for more than 100 cycles with only a slight increase in overpotential. For bare Li, the hysteresis quickly raised to over 600 mV and the cell failure happened within only 47 h. When setting both high current density and high capacity limit to 3 mA cm^{-2} and 2 mAh cm^{-2} , Li@P10 still demonstrated much longer cycle life and cycling stability, whereas the fluctuation and failure of the bare Li occurred in just 32 cycles (Figure S9, Supporting Information). Moreover, a superlong cycle life for more than 1000 h is demonstrated by Li@P10 (Figure S10, Supporting Information) at the current density of 0.5 mA cm^{-2} with the capacity of 1 mAh cm^{-2} . The overpotential of the protected Li was below 130 mV throughout the entire cycling period, which was significantly lower than the $\approx 350 \text{ mV}$ of bare Li at the end. The greatly extended life span of Li@P10 is attributed to an effective suppression of severe side reaction between metallic Li anode and electrolyte owing to the robust property of the artificial interface. Therefore, this work shows significantly improved performance over the previous works of alucone and Al_2O_3 coatings on Li,^[7] in terms of lower overpotential and extended cycling life under high current density and higher capacity. Promisingly, compared with the works from the literature, our polyurea coating on Li clearly exhibits excellent cycling stability and superlong life span over other protective layers (Table S1, Supporting Information). It is believed that the nitrogen-containing polar groups can homogenize the Li-ion flux and flexible polymer chains can buffer the volume expansion during stripping/plating. The coating thickness has been optimized by conducting different MLD cycles (5, 10, 25, and 50 cycles) of polyurea on Li foils and testing their corresponding electrochemical performance. As shown in Figure S12 in the Supporting Information, for 160 h of plating/stripping process, Li@P10 exhibited the most stable performance with the lowest overpotential among 5–50 MLD cycles. The excellent electrochemical performance can also be explained with the electrochemical impedance spectroscopy (EIS) analysis on the symmetric cells before and after 20 galvanostatic cycles. In Nyquist plots (Figure S11, Supporting

Information), high-frequency region can indicate the charge transfer resistance on the surface of Li and interfacial resistance at the interphase,^[5] and the value of each unit is obtained by fitting the equivalent circuit (Table S2, Supporting Information). Before cycling, larger resistance is detected in the symmetric cell using Li@P10 than that of bare Li due to the nonconductive property of polyurea. After 20 cycles, Li@P10 exhibited much smaller interfacial resistances in symmetric cells than bare Li, showing improved Li-ion conduction kinetics and the formation of a robust SEI under electrochemical cycling. EIS spectra of symmetric cells with different MLD cycles were also tested, in which Li@P25 and Li@P50 showed large interfacial resistance due to increased thickness. It is believed that few cycles of MLD (five cycles) are insufficient to prevent the severe side reaction between electrode and electrolyte. Moreover, thicker coatings (50 cycles) cause the large interfacial resistance (seen in Table S2 in the Supporting Information), leading to the fading of performances. Therefore, from EIS spectra the evidence of optimized thickness (10 cycles) is revealed from the interfacial resistance.

Both cells using bare Li and Li@P10 were disassembled and the electrodes were collected for SEM cross-section/top-view imaging after 20 stripping/plating cycles at a current density of 5 mA cm^{-2} and capacity of 1 mAh cm^{-2} to further explain the improved electrochemical performance. As shown in Figure 3a–c, a thick layer ($\approx 80 \mu\text{m}$) of porous “dead Li” was accumulated on the top of bare Li after 20 cycles. The huge volume expansion from the porous structure on the anode can lead to tremendous internal stress and cause several safety issues. By contrast, from Figure 3g–i, there was almost no porous layer observed in P10@Li, which indicates reduced “dead Li” formation during the stripping/plating process and will lead to higher CE. The top-view images from bare Li showed dense packing of irregular porous Li on the surface due to nonuniform Li deposition and stripping (Figure 3d–f). Moreover, long needle-like and mossy-like Li structures were also observed in both cross-section and top-view images as shown in Figure S16 in the Supporting Information. The large surface area of bare Li after cycling consumes a higher amount of electrolyte due to the side reactions with exposed Li, which could lead to a sharp decrease in the CE. Remarkably, as shown in Figure 3j–l, a smooth surface was observed on Li@P10 without any undesired mossy-like or needle-like Li. The Li foils after 20 cycles at 3 and 1 mA cm^{-2} were also characterized by SEM (Figures S13 and S14, Supporting Information). Similarly, compared with bare Li, coated Li foil still exhibited a much thinner layer of porous Li with a highly smooth surface, whereas a large amount of mossy-like Li was observed in the bare Li after cycling at 1 and 3 mA cm^{-2} (Figures S14 and S15, Supporting Information). Furthermore, a long dendrite was present in bare Li after cycling at 5 mA cm^{-2} (Figure S16, Supporting Information). For practical applications, the electrodes are expected to be operating for longer cycles. Thus, the electrodes after 650 plating/stripping cycles at the current density of 0.5 mA cm^{-2} with the capacity of 0.5 mAh cm^{-2} were also collected and characterized by SEM. After a long period of operation, a rough and porous “dead Li” layer accumulated on the bulk Li with a thickness of $\approx 180 \mu\text{m}$, whereas the volume of Li@P10 was still highly maintained with a thickness change of only $\approx 10 \mu\text{m}$

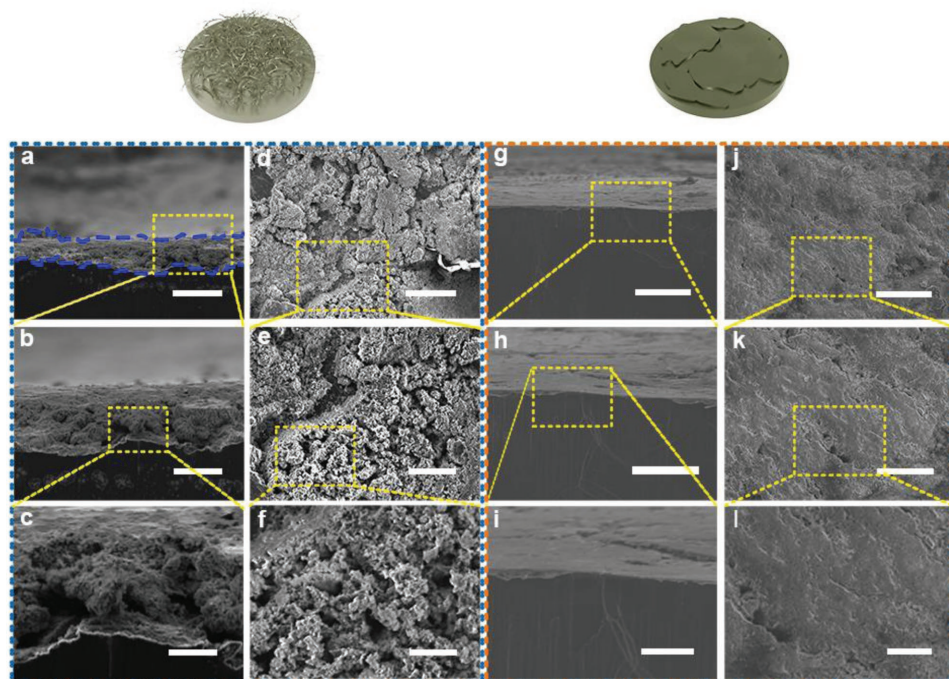


Figure 3. Surface morphologies for bare Li and Li@P10 after 20 cycles of stripping/plating. a–f) SEM images of cycled bare Li electrodes: a–c) cross-section and d–f) top-view images for an area of bare Li with different magnifications. g–l) Images of cycled Li@P10 electrodes: g–i) cross-section and j–l) top-view images for an area of Li@P10 with different magnifications. The lengths of scale bars are 100 μm for images (a), (d), (g), and (j), 50 μm for images (b), (e), (h), and (k), and 20 μm for images (c), (f), (i), and (l).

(Figures S17 and S18, Supporting Information). This morphology difference remarkably demonstrates that the polyurea film can ensure the operation of Li anodes with excellent cyclability. Therefore, it can be concluded that with proper polyurea coating on the surface, Li will undergo relatively uniform electrochemical stripping and plating with minimized production of dead Li.

To further understand the surface/interface change of the electrode, TOF-SIMS was conducted for the elemental distribution on the surface after 20 stripping/plating cycles for Li@P10. Strong signals of secondary ions were detected from hydrocarbon species (C_2H^- , C_4H^- , and C_6H^-) and carbon–nitrogen species (CN^- and NCO^-), which indicated that the composition of polyurea coating remains stable after the Li plating/stripping process (Figure 4a). The secondary ions of hydrocarbon species could be from both the polyurea chains and newly formed organic SEI layer (such as ROCO_2Li and ROLi), yet nitrogen-containing secondary ions, CN^- and NCO^- , were exclusively generated from the urea bonding of the polymer film. By consecutive sputtering of Cs^+ , a square area in the center with a depth of ≈ 7 nm was removed to obtain the depth profiles and mappings for secondary ions (Figure 4b,c). From the mappings after sputtering in the center area, the content of Li was notably higher than the outmost surface, while the contents of hydrocarbon and nitrogen-containing species were lower (Figure 4b). Depth profiles also showed the same trend of increasing Li content and decreasing hydrocarbon content and nitrogen–carbon species, which were consistent with the mappings before and after consecutive sputtering (Figure 4c). Interestingly, from the depth profile, we noticed that the SEI layer has a thickness of

≈ 7 nm (considering the sputter rate is 0.1 nm s^{-1}), which is thicker than the polyurea film before cycling. This observation suggests a newly formed SEI component upon cycling. The mapping images of secondary ions showed that the nitrogen-containing species were on the outermost surface, clearly demonstrating that the polyurea film remained on top, while the newly formed SEI component was formed between Li electrode and polyurea.

To further understand the chemical composition on the surface of the electrodes after 20 stripping/plating cycles, both bare Li and Li@P10 were collected from the cycled cells for XPS analysis. In the N 1s spectrum, the peak at 400.3 eV in Li@P10 can be assigned to amide/amine N in urea, whereas N 1s peak was not found in bare Li (Figure 4f,j). This result from N 1s spectrum was in good agreement with that from TOF-SIMS and confirmed that the robust polyurea coating remained on the surface as a composition of SEI. Compared with uncycled Li@P10, for cycled Li@P10 the major N species of amide/amine from polyurea still remained, while minor $\text{N}=\text{C}$ bond was not present that could be due to its reaction with active hydrogen species in electrolyte. The F 1s spectra showed peaks at 688.0 and 684.8 eV, corresponding to Li_xPF_y and LiF, respectively, in both bare Li and Li@P10 (Figure 4d,h). Li_xPF_y and LiF were normal components of SEI. However, much higher content of superior electronic insulating LiF was detected in Li@P10 than in bare Li. This is beneficial for SEI because LiF has an ultrahigh shear modulus (55.1 GPa) that can effectively suppress dendrite growth.^[23] In the O 1s spectrum for bare Li (Figure 4e), a peak at 530.2 eV corresponded to Li_2O and two peaks at 533.1 and 531.3 eV corresponded to C–O and C=O,

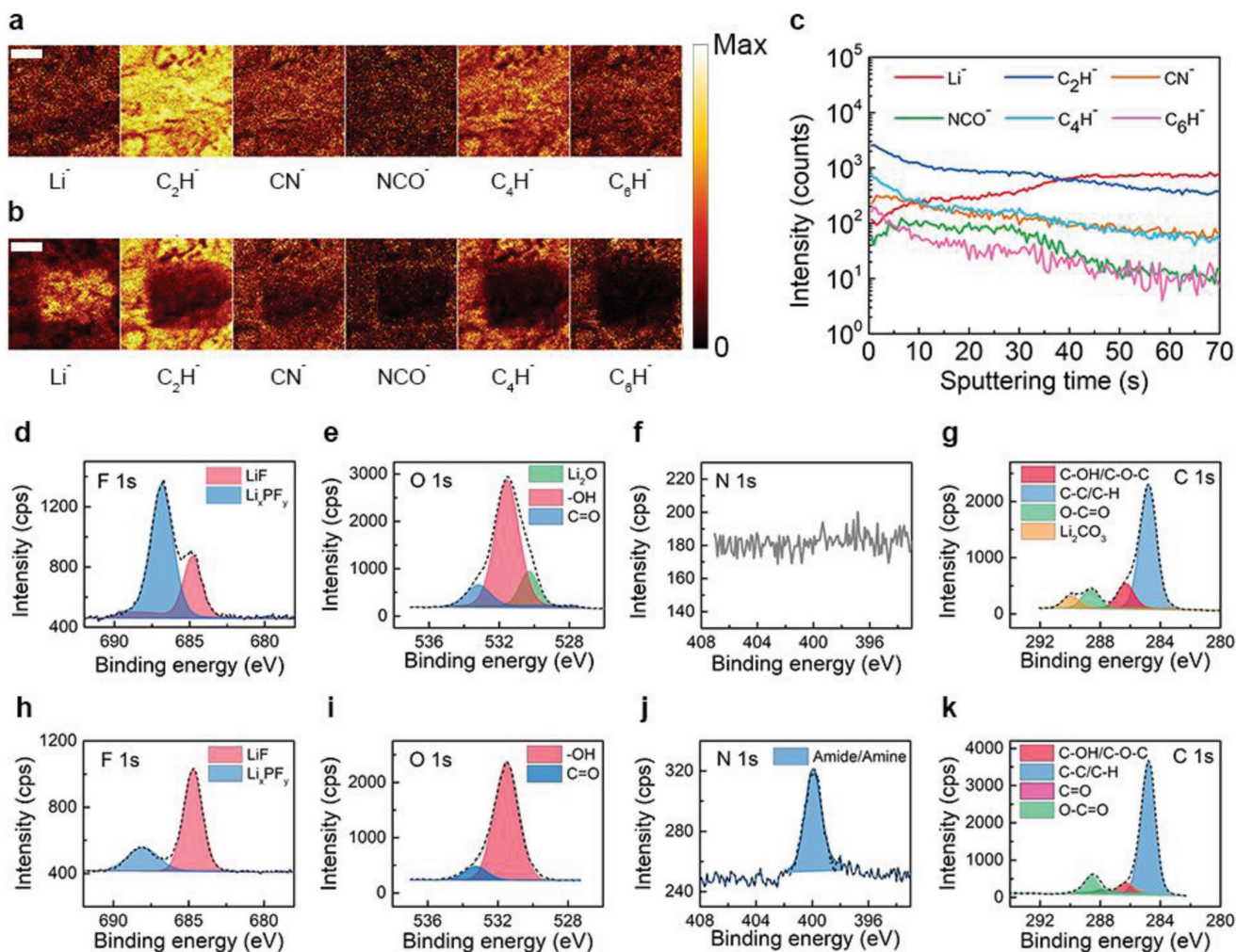


Figure 4. Characterization on the surface of electrodes after 20 plating/stripping cycles. a,b) TOF-SIMS secondary ion images of Li@P10 before (a) and after (b) Cs^+ consecutive sputtering for 70 s (the length of scale bar is 100 μm). c) Depth profile of various secondary ion species obtained by sputtering. d–k) XPS spectra for bare Li and Li@P10 electrodes: d) F 1s, e) O 1s, f) N 1s, and g) C 1s spectra of bare Li and h–k) corresponding spectra for Li@P10.

respectively, in the organic SEI components (such as $-\text{OCO}_2\text{Li}$ and $-\text{CO}_2\text{Li}$). Accordingly, in the O 1s spectrum for Li@P10 (Figure 4i), the same peaks at 533.1 and 531.3 eV were also present, and they could be from both the ordinary SEI as bare Li and organic polyurea film. There was no peak of Li_2O in Li@P10, which can be explained by the conversion of Li_2O to LiF under active F sources, such as F^- and PF_x^- . Multiple peaks from 284.4 to 289.9 eV were present in the C 1s spectra for bare Li (Figure 4g). These peaks corresponded to organic components and Li_2CO_3 of SEI for bare Li. For Li@P10, peaks were present at same positions with bare Li except that at 289.9 eV (Figure 4k), which indicates the absence of the thermodynamically unstable and brittle Li_2CO_3 .^[24] Furthermore, the hydrocarbon content and C–C bonding at 284.4 eV were significantly higher than those in bare Li, which may be attributed to the carbon skeleton of polyurea. From the XPS results, it is clearly shown that the thin polyurea film promotes the formation of LiF and reduces the formation of unstable SEI components (such as Li_2O and Li_2CO_3). The reason behind the stabilizing behavior of the coating could be explained by the

$-\text{NH}$ groups in polyurea, which provide strong interactions with PF_6^- from Li salt through hydrogen bonding ($\text{N}-\text{H}-\text{F}$) and can preferentially facilitate its decomposition to form LiF. Still, it is worth mentioning that the detailed chemistry and electrochemistry process on the coating upon cell operating still needs further exploration.

The performance of polyurea-coated Li was further investigated in full cells by coupling with LFP as cathode. LFP cells using bare Li and Li@P10 were cycled at a constant rate of 1 C to evaluate the influence of coating on Li anodes (Figure 5a). The areal LFP loading was 4.6 mg cm^{-2} and the corresponding current density was 0.8 mA cm^{-2} . Initially, LFP delivered a similar capacity with both bare Li and Li@P10. However, the capacity of the cell with bare Li decreased steadily from 130 to 90 mAh g^{-1} after 200 cycles, while highly improved capacity retention at 120 mAh g^{-1} of Li@P10 for 200 cycles was obtained. The charging/discharging profiles of the LFP cell with bare Li revealed higher voltage polarization than that with Li@P10 (Figure S19, Supporting Information). This suggested a smaller interfacial resistance in Li@P10 due to a robust SEI that

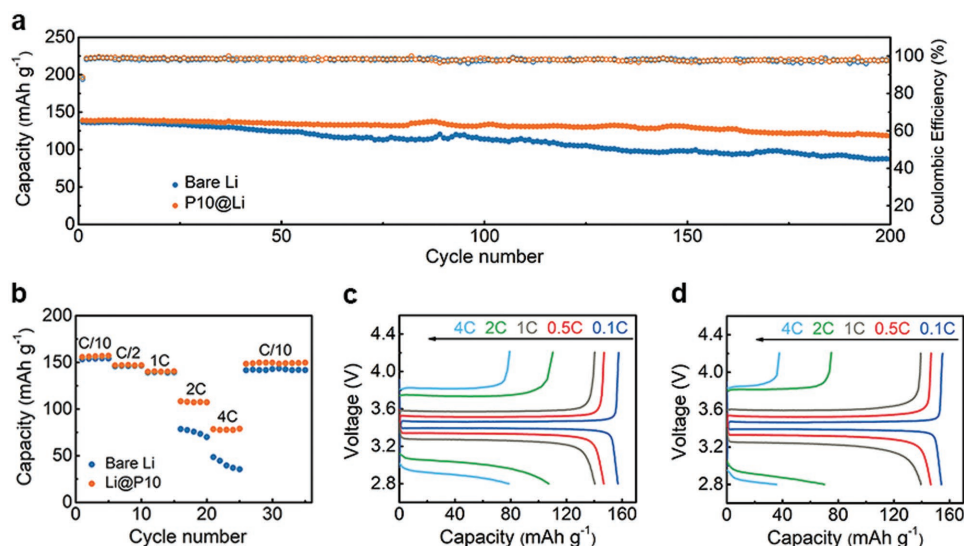


Figure 5. Electrochemical performance of Li/LFP cells using bare Li and Li@P10. a) Cycling performance at a rate of (1 C represents 170 mA g⁻¹). b) Rate capability for cycling from 0.1 C to 4 C. c) Galvanostatic charge/discharge voltage profiles on rate testing for Li@P10. d) Galvanostatic charge/discharge voltage profiles on rate testing for bare Li.

prevents the growth of dendritic/mossy Li and reduction of dead Li accumulation. The LFP cells were also cycled at different rates to study the influence of current density on Li anodes. Interestingly, although the capacities of the cell using Li@P10 were close to the capacities of bare Li at small rates, they were dramatically higher at 2 C and 4 C at high rates with a smaller degree of overpotential. The improved rate performance could be attributed to the polar groups in polyurea film that effectively directs a uniform distribution of Li-ion flux during plating/stripping and promotes faster ion transport kinetics.

In summary, highly controllable nanoscale polyurea coatings on metallic Li foil have been demonstrated for high-performance LMBs. After optimization of the film thickness, the Li with 10 cycles of polyurea coating has exhibited stable electrochemical plating/stripping performances and uniform Li deposition behaviors without the formation of undesired mossy/dendritic structures. An ultralong and stable cycling of more than 1000 h has been achieved for Li@P10 at a current density of 0.5 mA cm⁻². When increasing the current density to 3 mA cm⁻², the life span of Li@P10 is significantly extended by more than three times that of unprotected Li. In Li/LFP full cells, the Li@P10 has shown higher capacity retention and nearly 200% capacity of bare Li at a high rate of 4 C. A comprehensive study and deep understanding on the surface of electrodes using XPS and TOF-SIMS reveals the formation of stable SEI component with rich LiF and reduced Li₂O and Li₂CO₃ due to the positive effect from polyurea film. This study provides a novel and efficient approach to fabricate highly stable and safe Li-metal anodes with new insights for high-energy next-generation batteries.

Experimental Section

Electrode Preparation: Li foils were purchased from China Energy Lithium Co. Ltd and stored in an argon-filled glove box. Polishing was

conducted on Li foils to remove any oxide layers and cut into 3/8 in. diameter before coating and the thickness of Li foils was ≈250 μm. The synthesis procedure of MLD polyurea coating was modified from our reported work.^[20] The coating procedure was performed by an Arradiance GEMstar-8 ALD system, which was connected with the argon-filled glove box. Precursors were ethylenediamine (ED) and 1,4-phenylene diisocyanate (PDIC) provided by Sigma-Aldrich without further purification. Both ED and PDIC were held in separate external containers to isolate from air and moisture. ED was held at room temperature and PDIC was heated to 90 °C for a sufficient vapor pressure before MLD process. Polyurea coating was deposited on Li foils at 65 °C by alternative pulsing of ED and PDIC. A complete MLD cycle was described as ED pulse/purge/PDIC pulse/purge for periods of 0.1/30/1/30 s with a growth rate of ≈0.4 nm per cycle. Different number of cycles (5, 10, 25, and 50 cycles) were carried out on Li foils and denoted as Li@P5, Li@P10, Li@P25, and Li@P50, respectively.

Electrochemical Measurements: The as-prepared electrodes were used for the assembly of CR-2032 coin cells in the argon-filled glove box with oxygen and water levels lower than 1 ppm. Symmetric cells were assembled with configurations of Li/electrolyte-separator/Li and Li@P10/electrolyte-separator/Li@P10. In this work, Celgard 2400 polypropylene separators were used for all cells, and the electrolyte for each cell was 50 μL of 1 M LiPF₆ dissolved in 1:1:1 volume ratio of EC/DEC/DMC. Li plating/stripping performance was studied by a LAND eight-channel battery testing system. Electrochemical impedance spectroscopy was recorded on versatile multichannel potentiostat 3/Z (VMP3). To evaluate the influence of polyurea coating on full cell performances, Li-LiFePO₄ cells were assembled using either bare Li or Li@P10. To fabricate LFP cathode, a mixture of LiFePO₄, acetylene black, and poly(vinylidene difluoride) in a weight percentage of 80/10/10 was suspended in dimethylformamide as a slurry, casted on Al foil, and dried at 80 °C overnight. The areal loading of active material for the LFP cathodes was ≈4.6 mg cm⁻².

Characterization: A Hitachi 3400N environmental scanning electron microscope was used to obtain top-view and cross-section images after Li plating/stripping. The cells were disassembled in the argon-filled glove box and the anodes were washed with dimethyl carbonate to remove residual Li salts and electrolyte for all the post-cycling characterization. The Li foils were cut in half by a small blade for cross-section images. For XPS analysis, Li@P10 and bare Li foils were transferred from our Ar-filled glove box directly to the glove-box-connected XPS (Kratos AXIS Ultra Spectrometer) system for XPS analysis at the Surface Science Western. The XPS spectrometer was equipped with charging compensation for

accurate binding energy measurements and calibration. The TOF-SIMS tests were conducted using TOF-SIMS IV (ION-TOF GmbH, Germany) with a 25 keV bismuth liquid metal ion source with a base pressure at $\approx 10^{-8}$ mbar in the analysis chamber. The negative secondary ions were induced by the primary ion beam bombardment on the surface of Li electrodes. The analysis area was $334 \times 334 \mu\text{m}^2$. Depth profiles were obtained by sputtering ion beams of Cs^+ (3 keV) on square areas of $100 \times 100 \mu\text{m}^2$.

Supporting Information

Supporting Information is available from the Wiley Online Library or from the author.

Acknowledgements

Y.S. and Y.Z. contributed equally to this work. This work was funded by the Natural Science and Engineering Research Council of Canada (NSERC), the Canada Research Chair Program (CRC), the Canada Foundation for Innovation (CFI), the University of Western Ontario (UWO), and General Motors R&D Center. The authors also sincerely appreciate the help from Dr. Heng-Yong Nie on the discussion of TOF-SIMS analysis.

Conflict of Interest

The authors declare no conflict of interest.

Keywords

energy storage, interfaces, metallic lithium anodes, molecular-layer deposition

Received: October 9, 2018

Revised: November 6, 2018

Published online:

- [1] a) X. Gao, J. Wang, D. Zhang, K. Adair, K. Feng, N. Sun, H. Zheng, H. Shao, J. Zhong, Y. Ma, X. Sun, X. Sun, *J. Mater. Chem. A* **2017**, *5*, 25625; b) J. M. Tarascon, M. Armand, *Nature* **2001**, *414*, 359; c) J. Wang, H. Zhang, X. Lv, K. Nie, X. Gao, J. Zhong, X. Sun, *J. Mater. Sci.* **2016**, *51*, 6590.
- [2] a) R. Zhang, N.-W. Li, X.-B. Cheng, Y.-X. Yin, Q. Zhang, Y.-G. Guo, *Adv. Sci.* **2017**, *4*, 1600445; b) W. Xu, J. Wang, F. Ding, X. Chen, E. Nasybulin, Y. Zhang, J.-G. Zhang, *Energy Environ. Sci.* **2014**, *7*, 513; c) P. G. Bruce, S. A. Freunberger, L. J. Hardwick, J. M. Tarascon, *Nat. Mater.* **2012**, *11*, 19.
- [3] D. Lin, Y. Liu, Y. Cui, *Nat. Nanotechnol.* **2017**, *12*, 194.
- [4] P. G. Bruce, B. Scrosati, J. M. Tarascon, *Angew. Chem., Int. Ed.* **2008**, *47*, 2930.
- [5] D. Lin, Y. Liu, Z. Liang, H. W. Lee, J. Sun, H. Wang, K. Yan, J. Xie, Y. Cui, *Nat. Nanotechnol.* **2016**, *11*, 626.
- [6] J. Luo, R. C. Lee, J. T. Jin, Y. T. Weng, C. C. Fang, N. L. Wu, *Chem. Commun.* **2017**, *53*, 963.
- [7] Y. Zhao, L. V. Goncharova, Q. Sun, X. Li, A. Lushington, B. Wang, R. Li, F. Dai, M. Cai, X. Sun, *Small Methods* **2018**, *2*, 1700417.
- [8] a) S. Shi, P. Lu, Z. Liu, Y. Qi, L. G. Hector Jr., H. Li, S. J. Harris, *J. Am. Chem. Soc.* **2012**, *134*, 15476; b) D. Aurbach, E. Zinigrad, Y. Cohen, H. Teller, *Solid State Ionics* **2002**, *148*, 405; c) S.-P. Kim, A. C. T. v. Duin, V. B. Shenoy, *J. Power Sources* **2011**, *196*, 8590.
- [9] a) R. Younesi, G. M. Veith, P. Johansson, K. Edström, T. Vegge, *Energy Environ. Sci.* **2015**, *8*, 1905; b) N. W. Li, Y. X. Yin, J. Y. Li, C. H. Zhang, Y. G. Guo, *Adv. Sci.* **2017**, *4*, 1600400; c) Z. Li, J. Huang, B. Yann Liaw, V. Metzler, J. Zhang, *J. Power Sources* **2014**, *254*, 168.
- [10] a) D. Aurbach, E. Pollak, R. Elazari, G. Salitra, C. S. Kelley, J. Affinito, *J. Electrochem. Soc.* **2009**, *156*, A694; b) W. Li, H. Yao, K. Yan, G. Zheng, Z. Liang, Y. M. Chiang, Y. Cui, *Nat. Commun.* **2015**, *6*, 7436.
- [11] S. Zhang, Y. Liu, N. Zhang, K. Zhao, J. Yang, S. He, *J. Power Sources* **2016**, *329*, 1.
- [12] J. Luo, C.-C. Fang, N.-L. Wu, *Adv. Energy Mater.* **2018**, *8*, 1701482.
- [13] a) R. W. Johnson, A. Hultqvist, S. F. Bent, *Mater. Today* **2014**, *17*, 236; b) S. M. George, *Chem. Rev.* **2010**, *110*, 111; c) X. Meng, X. Q. Yang, X. Sun, *Adv. Mater.* **2012**, *24*, 3589.
- [14] a) Y. Zhao, L. V. Goncharova, A. Lushington, Q. Sun, H. Yadegari, B. Wang, W. Xiao, R. Li, X. Sun, *Adv. Mater.* **2017**, *29*, 1606663; b) L. Chen, J. G. Connell, A. Nie, Z. Huang, K. R. Zavadil, K. C. Klavetter, Y. Yuan, S. Sharifi-Asl, R. Shahbazian-Yassar, J. A. Libera, A. U. Mane, J. W. Elam, *J. Mater. Chem. A* **2017**, *5*, 12297.
- [15] E. Kazyak, K. N. Wood, N. P. Dasgupta, *Chem. Mater.* **2015**, *27*, 6457.
- [16] a) Y. Zhao, X. Sun, *ACS Energy Lett.* **2018**, *3*, 899; b) X. Meng, *J. Mater. Chem. A* **2017**, *5*, 18326; c) Q. Sun, K. C. Lau, D. Geng, X. Meng, *Batteries Supercaps* **2018**, *1*, 40.
- [17] a) H. Zhou, M. F. Toney, S. F. Bent, *Macromolecules* **2013**, *46*, 5638; b) N. M. Adamczyk, A. A. Dameron, S. M. George, *Langmuir* **2008**, *24*, 2081; c) Y. Du, S. M. George, *J. Phys. Chem. C* **2007**, *111*, 8509.
- [18] L. Chen, Z. Huang, R. Shahbazian-Yassar, J. A. Libera, K. C. Klavetter, K. R. Zavadil, J. W. Elam, *ACS Appl. Mater. Interfaces* **2018**, *10*, 7043.
- [19] L. Fan, H. L. Zhuang, W. Zhang, Y. Fu, Z. Liao, Y. Lu, *Adv. Energy Mater.* **2018**, *8*, 1703360.
- [20] A. Lushington, C. Langford, J. Liu, K. Nie, R. Li, X. Sun, J. Guo, X. Sun, *J. Phys. Chem. C* **2017**, *121*, 11757.
- [21] H.-Y. Nie, *J. Vac. Sci. Technol. B* **2016**, *34*, 030603.
- [22] a) P. W. Loscutt, H. Zhou, S. B. Clendinning, S. F. Bent, *ACS Nano* **2010**, *4*, 331; b) C. Prasittichai, H. Zhou, S. F. Bent, *ACS Appl. Mater. Interfaces* **2013**, *5*, 13391; c) U.-J. Choi, H. Kim, Y.-S. Park, J. S. Lee, *Bull. Korean Chem. Soc.* **2018**, *39*, 119.
- [23] J. Zhao, L. Liao, F. Shi, T. Lei, G. Chen, A. Pei, J. Sun, K. Yan, G. Zhou, J. Xie, C. Liu, Y. Li, Z. Liang, Z. Bao, Y. Cui, *J. Am. Chem. Soc.* **2017**, *139*, 11550.
- [24] K. Leung, F. Soto, K. Hankins, P. B. Balbuena, K. L. Harrison, *J. Phys. Chem. C* **2016**, *120*, 6302.